CEAS-GNC-2022-004

CEAS EuroGNC 2022
"Conference on Guidance, Navigation and Control"
3-5 May 2022 @ Technische Universität Berlin, Germany

Gaussian Progress Regression-based Disturbance Compensation Control for Urban Air Mobility

Dain Yoon Ph. D. Student, KAIST, Dept. of Aerospace Engineering, 34141, Daejeon, Republic of Korea. dainyoon@kaist.ac.kr

Chang-Hun Lee Assistant Professor, KAIST, Dept. of Aerospace Engineering, 34141, Daejeon, Republic of Korea. lckdgns@kaist.ac.kr

Min-Jea Tahk Emeritus Professor, KAIST, Dept. of Aerospace Engineering, 34141, Daejeon, Republic of Korea. mjtahk@kaist.ac.kr

ABSTRACT

This paper deals with a nonlinear attitude controller considering the disturbance rejection for urban air mobility (UAM). Using the disturbance observer-based control (DOBC) methodology, the proposed controller is constructed with a two-stage design procedure. The baseline control is established first by employing the time-scale separation approximation assumption and the feedback linearization approach, and then the Gaussian process regression (GPR) is augmented. Given the computational burden, the GP model is learned offline with a fixed-size training dataset. The GPR works as an adaptive law like the nonlinear disturbance observer. However, GPR can flexibly model the disturbance because the GPR describes the disturbance as a distribution over the functions. Furthermore, the control allocation method for the over-actuated system is presented to distribute the control command efficiently. Consequently, the proposed controller is validated with the numerical simulation under the various disturbance conditions such as model parameter uncertainties.

Keywords: Urban Air Mobility(UAM); Disturbance Rejection Control; Gaussian Process Regression; Feedback Linearization

1 Introduction

Nowadays, many people have been required for new transportation to smoothen traffic jams in an increasingly urbanized society. As the road capacity in the urban areas is expected to saturate, many countries prepare to utilize Urban Air Mobility (UAM), also called "air taxis," in their areas [1], [2]. Most of the research has been developing the electric vertical take-off and landing (eVTOL) UAM, which does not require the runway, for operating the system in the city. The eVTOL has been developed with different concepts such as multirotor (Volocopter 2X - Volocopter, EHang 184 - EHang), tiltrotor (Joby S4 - Joby Aviation, Butterfly - Hanwha Systems), and lift & cruise (Cora - Wisk Aero LLC). Recently, it has been discovered that the multirotor configuration is more efficient in hovering [2]. In addition, the multirotor structure is similar to unmanned aerial vehicles (UAVs), which have been extensively researched for the design of the controller. In this context, this paper mainly aims to design the adaptive controller for multirotor type UAM based on previous research for UAVs. This study could also be the base to design the autopilot for different types of UAM.

One of the challenging problems for UAM development is that it is typically characterized by high nonlinearities and contains unmodeled dynamics. Most nonlinear control systems, e.g., three-loop autopilot, utilize the system model parameters to make the control commands. Hence, the model uncertainties could degrade the tracking performance of the autopilot or even cause the mission failure. Moreover, UAM can be affected by external disturbances such as building wind because the objective region of the operation is generally a metropolitan area. In the past few years, some research activities have paid attention to these challenging issues. The authors in [3] proposed the active disturbance rejection controller with backstepping sliding-mode control methodology for quadrotor UAV considering the model uncertainties and external disturbances. A nonlinear disturbance-based controller in [4] was adopted for wind disturbance. Since much of the studies have been dealt with a small UAV, this paper focuses on the solution of the challenging issues considering the characteristics of UAM.

The two-loop autopilot is the minimal control structure that guarantees the desired dynamic characteristics [5]. This autopilot is based on the time-scale separation approximation and the feedback linearization control methodology combined with a specific form of the desired error dynamics. Since it is practical and straightforward to implement, the feedback linearization approach has been widely used for the autopilot design of various aerospace systems during the last few decades. The physical meaning and working principle of the autopilot that utilizes these concepts can be clearly understood. Furthermore, it could be designed with the nonlinear control approach [6] that does not require the gain scheduling method on the various operating points. On the other hand, the minimal control structure has a weakness against the model uncertainties or external disturbances. Therefore, when the two-loop topology is utilized, disturbance compensation techniques are also required to track the desired commands accurately and secure in their mission.

Accordingly, some papers proposed the autopilot with the disturbance rejection techniques for an accurate tracking performance even in the presence of parametric uncertainties or external disturbances like the wind. It has been reported that the three-loop topology, which contains the additional feedback loop to the minimal control structure, has robustness against the unmodeled dynamics [5]. This is because the integral term in the inner loop autopilot can counteract the disturbances as an adaptive law. The authors in [4, 7, 8] proposed the nonlinear disturbance observer-based control (DOBC) techniques for eliminating the adverse effects caused by the disturbances for various nonlinear systems. The time-delay approximation concept was utilized for observing and compensating the disturbance in [9, 10]. However, these parametric adaptive laws unavoidably have a transient region as the observations come from the equation consisting of the state variables and system parameters. When the control command is derived with an inaccurate estimate, it might degrade the performance of the baseline controller.

Gaussian process regression (GPR) has gained significant attention for handling the adverse effects of the disturbances and system identification. This data-driven control method can be a suitable treatment for the limitation of the parametric adaptive law as the inference takes place directly from the training datasets and corresponding GP model [11]. Besides, GPR can generally obtain a more flexible observation than the parametric methods under the sensor noise since it models the target value as the distribution over the functions. The view of the nonparametric method GPR requires less prior knowledge than the previous adaptive laws. Also, the unique advantage of GPR is that it provides the reliability values of the estimation model as to whether the obtained estimate is accurate or not. In [12], the authors conducted the GPR for estimating and regulating unknown disturbances related to the nonlinear friction and damping of the inverted pendulum. Reference [13] attempted to adopt the adaptive law, consisting of the modified GPR for online learning with a quaternion-based controller for the quadrotor system. Several related works to the online learning GPR in [14, 15]; however, it can be reached to the limitation by the computational burden for flight control systems as they are typically characterized as fast dynamics.

Consequently, this study aims to design the nonlinear two-loop autopilot with GPR to reduce the adverse effects of the disturbances while benefiting from the GPR with a fixed training dataset for real-

time implementation. The proposed autopilot is augmented by the two-loop baseline autopilot and the GPR adaptive scheme utilizing the DOBC technique due to practicality and efficiency in functioning [7]. Unlike previous research on disturbance rejection controllers, the baseline controller is built with the time-scale separation assumption and the feedback linearization methodology. They can present better insight into the physical sense and operational principle according to each control loop's desired tracking error dynamics. Corresponding to the procedure of the DOBC, there are two stages for autopilot construction; the baseline controller and GPR design. Firstly, the baseline controller is designed with specific forms of the error dynamics to make the resultant autopilot become the two-loop structure. Secondly, the GPR is designed for estimating and compensating the disturbance caused by the wind or system parameter variations.

The structure of this paper is as follows. In Section 2, the problem formulation is presented. In Section 3, the proposed autopilot design procedure is illustrated. In Section 4, the numerical simulation results are provided. Lastly, the conclusion of this study is offered in Section 5.

2 Problem Formulation

2.1 Nonlinear Dynamics Equations of UAM

In this section, nonlinear dynamic equations for the UAM system are described. Fig. 1 represents an octa-rotor VTOL type UAM, which is considered in this study. As described in Fig. 1, the UAM is assembled with eight co-axial rotors that are rotating in the opposite direction of each other. As described in Fig. 2, two coordinate frames are defined to describe the motion of the vehicle. The first frame is the North-East-Down (NED) frame $\{I\}$, which is called an inertial coordinate frame. The second frame is the body-fixed frame $\{B\}$ that the origin of the frame is attached to the center of gravity of the system. Furthermore, let us assume that the UAM has a rigid body. Also, we can ignore the aerodynamic force and body moment in the controller design stage since they are small enough.

According to the mentioned assumptions, the equations of motion for UAM can be derived from Newton's laws of motion. The velocity with respect to the body-fixed frame is written as

$$\dot{\boldsymbol{v}}_B = -\boldsymbol{\omega}_B \times \boldsymbol{v}_B + C_I^B \boldsymbol{g}_I + \frac{\Sigma \boldsymbol{F}_B}{m} \tag{1}$$

and the angular velocity in the body-fixed frame is defined as

$$\dot{\boldsymbol{\omega}}_B = I_B^{-1} \left(-\boldsymbol{\omega}_B \times I_B \boldsymbol{\omega}_B + \Sigma \boldsymbol{M}_B \right) \tag{2}$$

where the parameter m and the matrix $I_B = diag([I_{xx}, I_{yy}, I_{zz}])$ denote the mass and the moment of inertia of the flight vehicle, and the vector $\boldsymbol{g}_I = [0,0,g]^T$ represents the gravitational force in the inertial frame. The matrix C_I^B is the direction cosine matrix (DCM) rotating from the inertial frame to the body-fixed frame. The variables $\boldsymbol{v}_B = [u,v,w]^T$, and $\boldsymbol{\omega}_B = [p,q,r]^T$ represent the velocity and angular velocity with respect to the body-fixed frame. In addition, variables $\Sigma \boldsymbol{F}_B = [\Sigma F_x, \Sigma F_y, \Sigma F_z]^T$ and $\Sigma \boldsymbol{M}_B = [L,M,N]^T$ denote the total force and body moment.

The kinematic relationship equation between the Euler angle and angular rates can be written as

$$\dot{\phi} = p + q \sin\phi \tan\theta + r \cos\phi \tan\theta \tag{3}$$

$$\dot{\theta} = q \cos\phi - r \sin\phi \tag{4}$$

$$\dot{\psi} = q \sin\phi \sec\theta + r \cos\phi \sec\theta \tag{5}$$

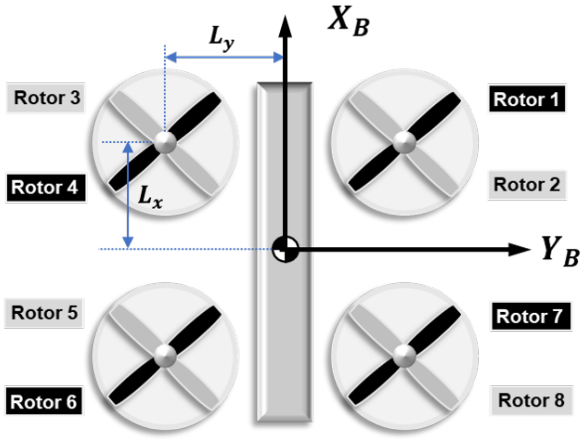

Fig. 1 The configuration of the UAM

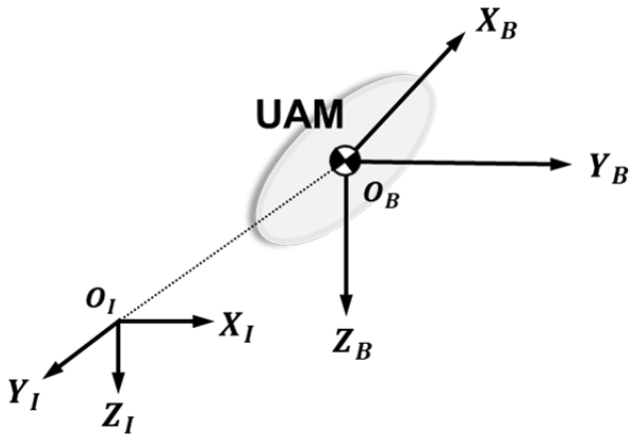

Fig. 2 Two coordinate frames

and the variables ϕ, θ, and ψ denote the roll, pitch, and yaw angles. Following the mentioned assumption, the total force is generated by each rotor and written as follows

$$\Sigma \boldsymbol{F}_B = \sum_{i=1}^{8} \boldsymbol{F}_{B,i} \tag{6}$$

$$\boldsymbol{F}_{B,i} \triangleq [0, 0, -\eta T_{\max,i} u_i]^T \tag{7}$$

and the total moment can be described as

$$\Sigma \boldsymbol{M}_B = \sum_{i=1}^{8} (\bar{\mathbf{x}}_i \times \boldsymbol{F}_{B,i} + \boldsymbol{R}_{B,i}) \tag{8}$$

$$\boldsymbol{R}_{B,i} \triangleq [0, 0, (-1)^{i+1} C_{q,i} T_i]^T \tag{9}$$

where the variables $\boldsymbol{F}_{B,i}$ and $\boldsymbol{R}_{B,i}$ represent the thrust force and moment caused by the i-th rotor. The variable u_i denotes the control input and the range of each rotor is in $(0,1)$. The distance from the i-th rotor to the origin of the body frame is written as $\bar{\mathbf{x}}_i = [L_x, L_y, 0]^T$, as shown in Fig. 1. The parameter $T_{max,i}$ provides the upper limit for the i-th rotor thrust force. The total force is not the exact sum of each thrust produced due to an interference effect of the co-axial rotor. Therefore, these characteristics of the co-axial rotor are modeled by an efficiency coefficient η and the counter-torque coefficient $C_{q,i}$.

2.2 Time-scale Separation Assumption

As shown in nonlinear dynamic equations (1-2), the motion of the UAM can be described by the velocity and angular velocity. The autopilot proposed in this paper chiefly concerns attitude control related to the angular velocity because it is a critical component for safe flight. From Eqs. (6-9), the control input variables have a direct effect on the body moment. It can be readily observed that the angular rate can be thought of as fast dynamics since the body moment induces the change in angular rate dynamics. In contrast, the Euler angles can be regarded as slow dynamic variables. The roll, pitch, and yaw angles are caused after the angular velocity generation as in Eqs. (3-5). These observations indicate that the complex dynamics can be decoupled into two dynamics mentioned above. Thus, the autopilot can be efficiently designed with a separation of the outer loop autopilot for Euler angles and the inner loop autopilot for angular velocity, as illustrated in Fig. 3.

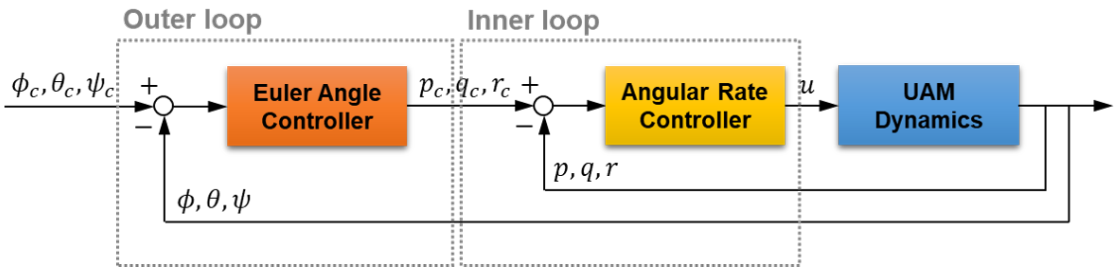

Fig. 3 Time-scale separation approximation-based control structure

3 Controller Design

In this section, the disturbance attenuation controller is designed by adopting the DOBC methodology in [7]. This structure is well known for its practical and effective implementation. The suggested disturbance rejection controller is established using a two-stage design method that includes the baseline controller and disturbance estimator design. The baseline controller is developed using time-scale separation assumption. Furthermore, the disturbance is treated as an external input at this design stage. Then, GPR is augmented to estimate and compensate for the disturbance to the baseline controller. Additionally, the control allocation algorithm is presented due to the distribution of the control input to each rotor. Thus, the structure of the entire autopilot described is designed through the following steps.

1) The baseline controller is designed using a two-loop feedback linearization methodology.
2) Gaussian process regression is constructed for estimating and compensating the disturbance.
3) The energy-effective control allocation matrix is also presented.

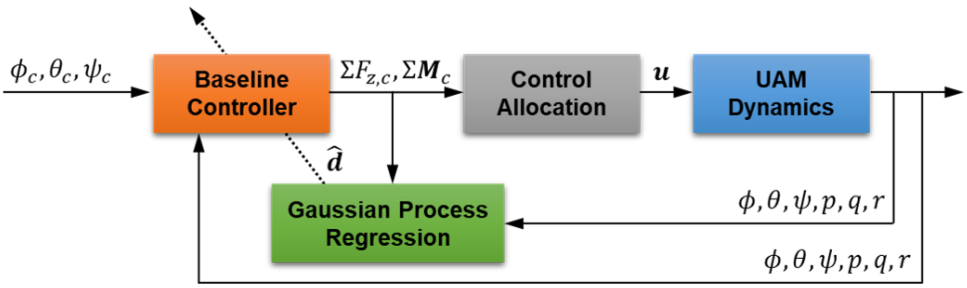

Fig. 4 Disturbance attenuation control structure

3.1 Baseline Controller

3.1.1 The outer loop controller

The baseline controller consists of two control loops: the outer loop controller for tracking given Euler angle commands (ϕ_c, θ_c, and ψ_c) and the inner loop controller for tracking desired angular rate values (p_c, q_c, and r_c). The outer loop is designed first based on the time-scale separation assumption. In this design step, the control commands are assumed to be slowly varying. The desired error dynamics are chosen as the first-order system in order to produce the resultant controller with the minimal control structure. The outer loop responses are characterized by the time constants: the design parameters τ_ϕ, τ_θ, and τ_ψ. The error convergence rates are related to these values.

$$\dot{\phi} = \frac{1}{\tau_\phi}(\phi_c - \phi) \tag{10}$$

$$\dot{\theta} = \frac{1}{\tau_\theta}(\theta_c - \theta) \tag{11}$$

$$\dot{\psi} = \frac{1}{\tau_\psi}(\psi_c - \psi) \tag{12}$$

From kinematic equations (3-5), and the above desired error dynamics equations (10-12), the angular velocity commands can be derived as

$$p_c = K_\phi(\phi_c - \phi) + p_b \tag{13}$$

$$q_c = K_\theta(\theta_c - \theta) + q_b \tag{14}$$

$$r_c = K_\psi(\psi_c - \psi) + r_b \tag{15}$$

where the parameters K_ϕ, K_θ, and K_ψ denote the control gains that are automatically determined as follows.

$$K_\phi = 1/\tau_\phi \tag{16}$$

$$K_\theta = 1/(\tau_\theta \cos\phi) \tag{17}$$

$$K_\psi = 1/(\tau_\psi \cos\phi \sec\theta) \tag{18}$$

The first terms of Eqs. (13-15) have the form of proportional feedback control for tracking the desired error dynamics. Additionally, the second terms that are written as the bias control terms p_b, q_b, and r_b act for maintaining the trim conditions, and they have the forms as described below.

$$p_b = -q\sin\phi\tan\theta - r\cos\phi\tan\theta \tag{19}$$

$$q_b = r\tan\phi \tag{20}$$

$$r_b = -q\tan\phi \tag{21}$$

3.1.2 The inner loop controller

While developing the inner loop controller, the disturbances are considered as the external input d_p, d_q, and d_r as follows.

$$\dot{p} = \frac{(I_{yy} - I_{zz})}{I_{xx}} qr + \frac{L}{I_{xx}} + d_p \tag{22}$$

$$\dot{q} = \frac{(I_{zz} - I_{xx})}{I_{yy}} pr + \frac{M}{I_{yy}} + d_q \tag{23}$$

$$\dot{r} = \frac{(I_{yy} - I_{xx})}{I_{zz}} pq + \frac{N}{I_{zz}} + d_r \tag{24}$$

As shown in Fig. 3, the purpose of the inner loop is to track the commands provided from the outer loop. According to the time-scale separation assumption, the derivative of the given rate commands can be considered as zero ($\dot{\boldsymbol{\omega}}_{B,c} \approx 0$). Thus, the desired error dynamics for tracking the desired values using the minimal control structure are chosen by the first-order system as follows.

$$\dot{p} = \frac{1}{\tau_p} (p_c - p) \tag{25}$$

$$\dot{q} = \frac{1}{\tau_q} (q_c - q) \tag{26}$$

$$\dot{r} = \frac{1}{\tau_r} (r_c - r) \tag{27}$$

From Eq. (2) and the above desired error dynamics in Eqs. (25-27), the moment commands can be obtained as

$$L_c = K_p (p_c - p) + L_b - I_{xx} d_p \tag{28}$$

$$M_c = K_q (q_c - q) + M_b - I_{yy} d_q \tag{29}$$

$$N_c = K_r (r_c - r) + N_b - I_{zz} d_r \tag{30}$$

where the parameters K_p, K_q, and K_r stand for the control gain of the inner loop, and they are derived as follows.

$$K_p = 1/\tau_p \tag{31}$$

$$K_q = 1/\tau_q \tag{32}$$

$$K_r = 1/\tau_r \tag{33}$$

The first terms of Eqs. (28-30) denote the proportional feedback control command, whereas the second terms L_b, M_b, and N_b represent the control command to maintain the trim conditions.

$$L_b = (I_{yy} - I_{zz}) qr \tag{34}$$

$$M_b = (I_{zz} - I_{xx}) pr \tag{35}$$

$$N_b = (I_{yy} - I_{xx}) pq \tag{36}$$

Moreover, the third terms in Eqs. (28-30) are for the compensation of the disturbance. In general, it is impossible to measure the actual values of d_p, d_q, and d_r. Hence, the estimate using adaptive law should be required as described in Fig. 4, and the next section will cover the design of the GPR.

3.2 Gaussian Process Regression

This subsection describes the disturbance estimation algorithm to treat the problem during the operation of UAM by adopting the Bayesian approach (i.e., GPR). The GPR can provide the estimate as a distribution over the function, so it has much more flexibility than the previous parametric adaptive laws for observing the unmodeled dynamics. The GP model trains the model with a predefined training dataset due to reducing the computational overload. The explanation of the design procedure for GPR is exemplarily given to pitch dynamics for conciseness. The GPR for roll and yaw dynamics can be constructed similarly. The structure of the training dataset is as

$$\mathscr{D}_q = \left\{X_q, \boldsymbol{y}_q\right\} = \left\{\boldsymbol{x}_q^{(i)}, y_q^{(i)} | i = 1, \cdots, N\right\} \tag{37}$$

where the vector $\boldsymbol{x}_q^{(i)}$ is the i-th input data that is composed of the velocity, Euler angles, and the attitude angle commands as

$$\boldsymbol{x}_q^{(i)} = \left[u^{(i)}, v^{(i)}, w^{(i)}, \phi^{(i)}, \theta^{(i)}, \psi^{(i)}, \theta_c^{(i)}\right]^T \tag{38}$$

and the i-th output data of the training dataset containing the measurement noise ε_q with standard deviation σ_q can be written as follows.

$$y_q^{(i)} = d_q\left(\boldsymbol{x}_q^{(i)}\right) + \varepsilon_q \tag{39}$$

$$\varepsilon_q \sim \mathscr{N}(0, \sigma_q^2) \tag{40}$$

The dataset is collected in the operation range during the data acquisition phase, according to the structure mentioned above. Typically, the output data are unknown, so the numerical differentiation is taken to calculate the disturbance by utilizing the modification of Eq. (23) as below. The estimation error could be thought of as a component of the measurement noise.

$$y_q^{(i)} \approx \dot{q} - \frac{(I_{zz} - I_{xx})}{I_{yy}} pr - \frac{M}{I_{yy}} \tag{41}$$

The prior GP model is composed of the mean function and covariance function that also called the kernel. The prior mean function is chosen as zero because there is no disturbance information. The prior covariance function employs the squared exponential (SE) kernel, which has an excellent property that provides the precise modeling for any arbitrary continuous function [16].

$$d_{gp,q} \sim GP(0, k_{SE}(\boldsymbol{x}, \boldsymbol{x}')) \tag{42}$$

where

$$k_{SE}\left(\boldsymbol{x}, \boldsymbol{x}'\right) = \sigma_f^2 \exp\left(-\frac{(\boldsymbol{x} - \boldsymbol{x}')^T (\boldsymbol{x} - \boldsymbol{x}')}{2l^2}\right) \tag{43}$$

The vector $\psi_{SE} \triangleq \left[\sigma_f^2, l\right]^T$ consists of the hyperparameters that represent the characteristics of the kernel, and they can be optimized by maximizing the log marginal likelihood as

$$\psi_{SE,q}^* = \arg\max_{\psi_{SE}} \log p\left(\boldsymbol{y}_q | X_q, \psi_{SE}\right) \tag{44}$$

where

$$\log p\left(\boldsymbol{y}_q | X_q, \psi_{SE}\right) = \frac{1}{2}\left(\boldsymbol{y}_q^T K^{-1} \boldsymbol{y}_q - \log\det K - N\log(2\pi)\right) \tag{45}$$

with kernel evaluations for all pairs of training data that can be written as follows.

$$K = \begin{bmatrix} k\left(\boldsymbol{x}_q^{(1)}, \boldsymbol{x}_q^{(1)}\right) & \cdots & k\left(\boldsymbol{x}_q^{(1)}, \boldsymbol{x}_q^{(N)}\right) \\ \vdots & \ddots & \vdots \\ k\left(\boldsymbol{x}_q^{(N)}, \boldsymbol{x}_q^{(1)}\right) & \cdots & k\left(\boldsymbol{x}_q^{(N)}, \boldsymbol{x}_q^{(N)}\right) \end{bmatrix} \tag{46}$$

When the test point $\boldsymbol{x}_q^*$ is given, the posterior mean and the variance function according to the training dataset and the prior GP model can be calculated by the following joint Gaussian distribution.

$$\begin{bmatrix} d_{gp,q}\left(\boldsymbol{x}_q^*\right) \\ \boldsymbol{y}_q \end{bmatrix} \sim N\left(0, \begin{bmatrix} k^* & \boldsymbol{k}^T \\ \boldsymbol{k} & K + \sigma_q^2 I_N \end{bmatrix}\right) \tag{47}$$

where

$$k^* = k\left(\boldsymbol{x}_q^*, \boldsymbol{x}_q^*\right) \tag{48}$$

$$\boldsymbol{k} = \left[k\left(\boldsymbol{x}_q^{(1)}, \boldsymbol{x}_q^*\right), \cdots, k\left(\boldsymbol{x}_q^{(N)}, \boldsymbol{x}_q^*\right)\right]^T \tag{49}$$

Then, the posterior mean can be obtained by

$$\mu_q\left(\boldsymbol{x}_q^*\right) = \mathbb{E}\left[d_{gp,q}\left(\boldsymbol{x}_q^*\right) \middle| X_q, \boldsymbol{y}_q\right] = \boldsymbol{k}^T\left(K^{-1} + \sigma_q^2 I_N\right)^{-1} \boldsymbol{y}_q \tag{50}$$

and the posterior variance can be represented as follows.

$$\sigma_q\left(\boldsymbol{x}_q^*\right) = \mathbb{V}\left[d_{gp,q}\left(\boldsymbol{x}_q^*\right) \middle| X_q, \boldsymbol{y}_q\right] = k^* - \boldsymbol{k}^T\left(K + \sigma_q^2 I_N\right)^{-1} \boldsymbol{k} \tag{51}$$

Consequently, the estimate for the test point is given by a probabilistic model, the posterior mean function, as $\hat{d}_q = \mu_q\left(\boldsymbol{x}_q^*\right)$. The posterior mean function is employed for disturbance compensation by replacing the unknown disturbance in Eq. (29). Additionally, the variance function can present the reliability of the estimated model.

3.3 Control Allocation Logic

Since this study considers the UAM with eight co-axial rotors, which is an over-actuated system, the control allocation technique is required to distribute the control command appropriately. From Eqs. (6-9), the relationships between the command input variables u and the total force and moment acting on the flight vehicle can be briefly written with the matrix Ψ as follows.

$$\begin{bmatrix} \Sigma F_z \\ \Sigma \boldsymbol{M}_B \end{bmatrix} \triangleq \Psi \boldsymbol{u} \tag{52}$$

For an over-actuated system, the concept of Moore-Penrose pseudo-inverse can be utilized to minimize the energy of the control action [17]. Finally, the rotor throttle input $\boldsymbol{u}$, which considers the control energy efficiency, can be calculated as

$$\boldsymbol{u} = \Psi^+ \begin{bmatrix} \Sigma F_{z,c} \\ \Sigma \boldsymbol{M}_c \end{bmatrix} \tag{53}$$

where

$$\Psi^+ = \Psi^T\left(\Psi\Psi^T\right)^{-1} \tag{54}$$

4 Simulation Study

In this section, the performance of the proposed disturbance rejection controller is demonstrated through the numerical simulations under the presence of the disturbance and system parameter uncertainties. As described in Eqs. (22-24), the disturbance caused by wind or system parameter variation is assumed to affect the inner loop directly. The system model parameters are presented in Tab. 1, and the design parameters for each autopilot are chosen as follows.

$$\tau_\phi = 0.5(sec), \quad \tau_\theta = 0.5\,(\text{sec}), \quad \tau_\psi = 0.5\,(\text{sec}) \tag{55}$$

$$\tau_p = 0.1(sec), \quad \tau_q = 0.1\,(\text{sec}), \quad \tau_r = 0.1\,(\text{sec}) \tag{56}$$

The training data for offline GP learning is collected in the operating region that is -30(deg) to 30(deg) in Euler angles for each test case. After gathering the training data, the fifty pair (i.e., $N = 50$ in Eq. (37)) of data is randomly chosen for reducing the computational burden.

Table 1 The UAM model parameters used in this study

Parameter	Description	Value	Unit
m	Mass of the UAM	320	(kg)
I_B	Moment of inertia of the UAM	$diag\,([40, 240, 220])$	$(\text{kg} \cdot \text{m}^2)$
(L_x, L_y)	Distance from the rotor to the CG	$(2, 1)$	(m)
τ_a	Time constant of the actuator	0.01	(sec)

Firstly, the controller is tested with a form of constant disturbances, which has values $d_p = 50(\text{deg/s}^2)$, $d_q = 50(\text{deg/s}^2)$, and $d_r = 0(\text{deg/s}^2)$. Slowly varying wind or disturbance caused by uncertainty in the center of gravity [8] could be considered similar in this case. The response of the attitude controller with step command ($\Omega_c = [10, 10, 0]^T(\text{deg})$) is presented in Fig. 5(a). Also, the nominal response of the baseline controller, as well as the response of the baseline controller without the disturbance rejection algorithm, is attached for analyzing the performance. Figure 5(a) indicates that bias type error appears when any disturbance rejection algorithm is not applied. As shown in Fig. 5(b), the GPR can estimate given disturbance accurately, including the transient phase, unlike the other methods such as the nonlinear disturbance observer (green-dashed line). Thus, the proposed Euler angle controller for the UAM can accurately track the commands similar to the nominal response even in the presence of the disturbances.

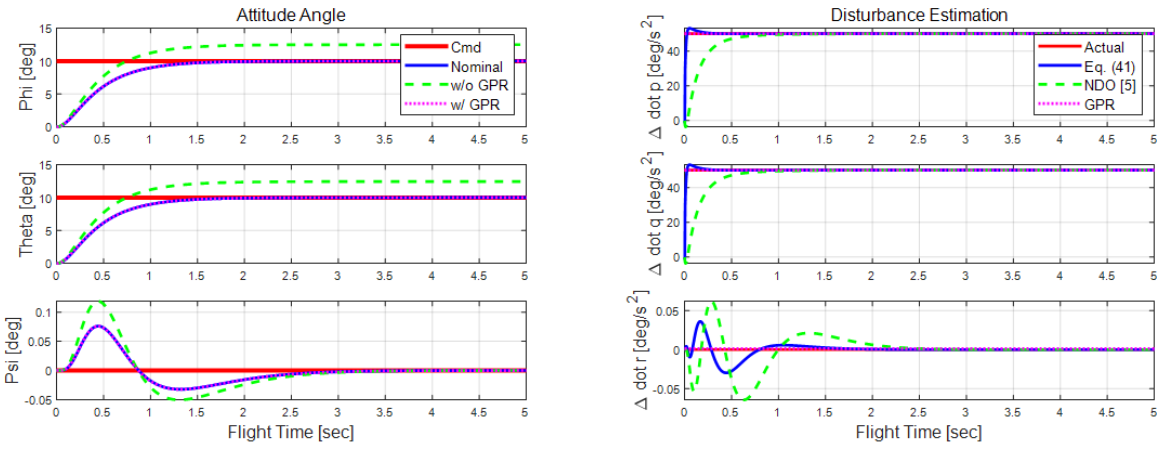

(a) Attitude Controller Response

(b) Disturbance Estimation Performance

Fig. 5 Disturbance rejection performance under case 1; disturbance with a form of constant

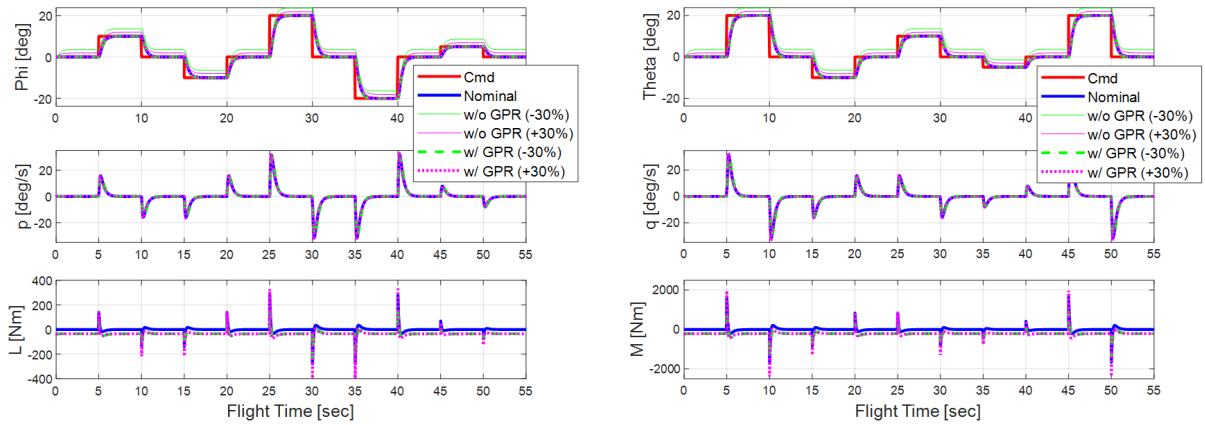

(a) Roll Angle Control Response

(b) Pitch Angle Control Response

Fig. 6 Disturbance rejection performance under case 2; constant disturbance, and uncertainties in MOI

Secondly, the proposed controller is tested by imposing various step commands under the constant disturbance, which is the same in the first case and the model uncertainty. In this case, the value of the moment of inertia is considered to differ from the actual as $\pm 30\%$. Figure 6 represents that the designed system can provide robust tracking performance under given conditions. Furthermore, the disturbance rejection performance of GPR is well verified. Although there is a slight difference in the transient phase when compared to the nominal response, the primary issue, a bias type error, is completely controlled. According to the findings, even in the presence of these disturbances, the suggested disturbance rejection algorithm would deliver adequate performance in these disturbances conditions.

5 Conclusion

Utilizing the DOBC concept, the nonlinear attitude controller and the GPR are designed and combined to tackle the negative effect caused by wind and system parameter uncertainties for the UAM. The baseline controller is designed using the feedback linearization methods (i.e., a two-loop controller that is the minimal control structure). The augmented GPR works as an adaptive law like the disturbance observer to compensate for the disturbance actively. The GPR model is trained offline with a fixed dataset to reduce the computational effort while implementing. The control allocation mechanism is also provided to produce the thrust force efficiently. In contrast to the prior parametric adaptive law, the numerical simulation results demonstrate that the designed GPR adequately predicts the disturbance, including the transient region. Thus, the suggested controller offered satisfactory tracking performance even in the presence of a form of constant disturbance and the system parameter uncertainties. As a result, the described disturbance rejection attitude controller can address the problems related to the disturbance of UAM autopilot.

Acknowledgments

This research was supported by Unmanned Vehicles Core Technology Research and Development Program through the National Research Foundation of Korea and Unmanned Vehicle Advanced Research Center funded by the Ministry of Science and ICT, the Republic of Korea (No.NRF-2020M3C1C1A0108 316111).

References

[1] Nicolas Runge, Ryan Twedt, Wade Olson, Sterling Berg, Isaac Smithee, Todd Letcher, and Marco Ciarcià. Design, development, and testing of an autonomous multirotor for personal transportation. In *Proceedings of the 2020 USCToMM Symposium on Mechanical Systems and Robotics*, volume 83, page 53. Springer Nature, 2020.

[2] Alessandro Bacchini and Enrico Cestino. Electric vtol configurations comparison. *Aerospace*, 6(3):26, 2019.

[3] Lin-Xing Xu, Hong-Jun Ma, Dong Guo, An-Huan Xie, and Da-Lei Song. Backstepping sliding-mode and cascade active disturbance rejection control for a quadrotor uav. *IEEE/ASME Transactions on Mechatronics*, 25(6):2743–2753, 2020.

[4] Fuyang Chen, Wen Lei, Kangkang Zhang, Gang Tao, and Bin Jiang. A novel nonlinear resilient control for a quadrotor uav via backstepping control and nonlinear disturbance observer. *Nonlinear Dynamics*, 85(2):1281–1295, 2016.

[5] Chang-Hun Lee, Shaoming He, and Ju-Hyeon Hong. Investigation on physical meaning of three-loop autopilot. *International Journal of Control, Automation and Systems*, 18(11):2709–2720, 2020.

[6] Chang-Hun Lee, Byung-Eul Jun, and Jin-Ik Lee. Connections between linear and nonlinear missile autopilots via three-loop topology. *Journal of Guidance, Control, and Dynamics*, 39(6):1426–1432, 2016.

[7] Wen-Hua Chen. Disturbance observer based control for nonlinear systems. *IEEE/ASME transactions on mechatronics*, 9(4):706–710, 2004.

[8] Dain Yoon, Young-Won Kim, Taeho Jeong, Chang-Hun Lee, and Min-Jea Tahk. A nonlinear disturbance observer-based adaptive controller considering cg variation of urban aerial mobility. In *2021 29th Mediterranean Conference on Control and Automation (MED)*, pages 991–996. IEEE, 2021.

[9] Chang-Hun Lee, Tae-Hun Kim, and Min-Jea Tahk. Agile missile autopilot design using nonlinear backstepping control with time-delay adaptation. *Transactions of the Japan Society for Aeronautical and Space Sciences*, 57(1):9–20, 2014.

[10] Chang-Hun Lee, Byung-Eul Jun, Jin-Ik Lee, and Min-Jea Tahk. Nonlinear missile autopilot design via three loop topology and time-delay adaptation scheme. In *2013 13th International Conference on Control, Automation and Systems (ICCAS 2013)*, pages 50–54. IEEE, 2013.

[11] Zhe Hu, Peigen Sun, and Jia Pan. Three-dimensional deformable object manipulation using fast online gaussian process regression. *IEEE Robotics and Automation Letters*, 3(2):979–986, 2018.

[12] Harald Aschemann and Cristina Tarín. Gaussian process based disturbance compensation for an inverted pendulum. *IFAC-PapersOnLine*, 53(2):8732–8737, 2020.

[13] Ruping Cen, Tao Jiang, and Pan Tang. Modified gaussian process regression based adaptive control for quadrotors. *Aerospace Science and Technology*, 110:106483, 2021.

[14] Jonas Umlauft and Sandra Hirche. Feedback linearization based on gaussian processes with event-triggered online learning. *IEEE Transactions on Automatic Control*, 65(10):4154–4169, 2019.

[15] Daniel Bergmann, Michael Buchholz, Jens Niemeyer, Jörg Remele, and Knut Graichen. Gaussian process regression for nonlinear time-varying system identification. In *2018 IEEE Conference on Decision and Control (CDC)*, pages 3025–3031. IEEE, 2018.

[16] David Duvenaud. *Automatic model construction with Gaussian processes*. PhD thesis, University of Cambridge, 2014.

[17] Tor A Johansen and Thor I Fossen. Control allocation—a survey. *Automatica*, 49(5):1087–1103, 2013.